Received: 4 April 2021 | Revised: 21 August 2021 | Accepted: 23 August 2021

DOI: 10.1002/mrm.29004

TECHNICAL NOTE

Magnetic Resonance in Medicine

Three-dimensional quantification of circulation using finite-element methods in four-dimensional flow MR data of the thoracic aorta

Julio Sotelo[1,2,3] | **Malenka M. Bissell**[4] | **Yaxin Jiang**[4] | **Hernan Mella**[2,3,5] | **Joaquín Mura**[3,6] | **Sergio Uribe**[2,3,7,8]

[1]School of Biomedical Engineering, Universidad de Valparaíso, Valparaíso, Chile

[2]Biomedical Imaging Center, Pontificia Universidad Católica de Chile, Santiago, Chile

[3]Millennium Nucleus in Cardiovascular Magnetic Resonance, CardioMR, Santiago, Chile

[4]Department of Biomedical Imaging Science, Leeds Institute of Cardiovascular and Metabolic Medicine, University of Leeds, Leeds, UK

[5]Department of Electrical Engineering, Pontificia Universidad Católica de Chile, Santiago, Chile

[6]Department of Mechanical Engineering, Universidad Técnica Federico Santa María, Santiago, Chile

[7]Department of Radiology, School of Medicine, Pontificia Universidad Católica de Chile, Santiago, Chile

[8]Institute for Biological and Medical Engineering, Schools of Engineering, Medicine and Biological Sciences, Pontificia Universidad Católica de Chile, Santiago, Chile

Correspondence
Julio Sotelo, School of Biomedical Engineering, Universidad de Valparaíso, General Cruz 222, Valparaíso, Chile.
Email: Julio.sotelo@uv.cl

Funding information
Fondo Nacional de Desarrollo Científico y Tecnológico (Iniciación), Grant/Award Number: 11200481; Millenium Nucleus in Cardiovascular Magnetic Resonance, Grant/Award Number: NCN17_129; Fondo Nacional de Desarrollo Científico y Tecnológico (Regular), Grant/Award Number: 1181057; Agencia Nacional de Investigación y Desarrollo (PhD Scholarship), Grant/Award Number: 21170592; Fondo Nacional de Desarrollo Científico y Tecnológico (Postdoc), Grant/Award Number: 3170737

Purpose: Three-dimensional (3D) quantification of circulation using a Finite Elements methodology.

Methods: We validate our 3D method using an in-silico arch model, for different mesh resolutions, image resolution and noise levels, and we compared this with a currently used 2D method. Finally, we evaluated the application of our methodology in 4D Flow MRI data of ascending aorta of six healthy volunteers, and six bicuspid aortic valve (BAV) patients, three with right and three with left handed flow, at peak systole. The in-vivo data was compared using a Mann-Whitney U-test between volunteers and patients (right and left handed flow).

Results: The robustness of our method throughout different image resolutions and noise levels showed subestimation of circulation less than 45 cm^2/s in comparison with the 55cm^2/s generated by the current 2D method. The circulation (mean ± SD) of the healthy volunteer group was 13.83 ± 28.78 cm^2/s, in BAV patients with right-handed flow 724.37 ± 317.53 cm^2/s, and BAV patients with left-handed flow −480.99 ± 387.29 cm^2/s. There were significant differences between healthy volunteers and BAV patients groups (P-value < .01), and also between BAV patients with a right-handed or left-handed helical flow and healthy volunteers (P-value < .01).

Conclusion: We propose a novel 3D formulation to estimate the circulation in the thoracic aorta, which can be used to assess the differences between normal and diseased hemodynamic from 4D-Flow MRI data. This method also can

correctly differentiate between the visually seen right- and left-handed helical flow, which suggests that this approach may have high clinical sensitivity, but requires confirmation in longitudinal studies with a large cohort.

KEYWORDS
4D flow MRI, bicuspid aortic valve, circulation, finite elements, hemodynamic parameters

1 | INTRODUCTION

Bicuspid aortic valve (BAV) is the most common congenital heart defect,[1] being present in at least 1% of the population, with higher prevalence in white population and males (3:1).[2,3] Dilatation of the ascending aorta (AAo) develops in approximately 40% of BAV patients.[1] It is associated with an increased risk of aortic dissection, rupture, and sudden death.[4] However, patients' risk prediction is complex, because it depends on multiple genetic, histological, mechanical, and hemodynamics factors.[1] Therefore, there is a need to better understand the mechanisms influencing the progression of these structural changes, which may allow the development of prognostic models for risk assessment, the need of surgical correction, and pre- and post-operative monitoring.[5,6]

Cardiovascular hemodynamic parameters quantified from four-dimensional (4D)-flow MRI bring new insights into complex flow characteristic in BAV patients.[7] Recent studies have provided strong evidence that rotational blood flow hemodynamics in the AAo of BAV patients is associated with histological and proteolytic changes of the aortic wall, which may lead to aortic focal flow-induced vascular remodeling.[8,9] Hemodynamics parameters such as eccentricity and wall shear stress (WSS) show the potential to characterize these complex flow pattern.[10-12] Moreover, the circumferential component of WSS can indirectly capture the rotational behavior of the blood flow characteristics in these patients, showing great advantages over 2D methods.[13] The circulation is a metric used in fluid dynamics to quantify the rotational components of flow and is usually analyzed in 2D cross-sections using Stoke's Theorem.[14] This parameter has only been used on 2D reformatted 4D flow MRI data.[15-18] In a recent work proposed by Hattori et al,[18] they showed the relevance of analyzing the circulation to characterize the morphology of patients with BAV, using 4D flow obtained in controlled experiments from in-vitro data. However, it is well known that the generation of this cross-section is highly operator dependent, that can induce overlap of planes (particularly in curved or intrincated geometries) and can assess only to local information.[13] We hypothesize that the 3D circulation of the flow can provide valuable information to better understand the hemodynamics alteration in BAV patients.

The purpose of this work is the development and validation of a methodology based on finite elements (FE) to calculate the circulation in a 3D domain, giving information of both the rotation and the helical behavior of the blood flow in the ascending aorta of BAV patients. We use an in-silico arch model under different resolutions and noise levels to validate our method. Moreover, to show the clinical application of this metric, we calculated this parameter in the AAo of six healthy volunteers and six BAV patients, three with right- and three with left-handed flow rotation.

2 | METHODS

2.1 | Quantification of 3D circulation

The circulation (Γ) was defined as the integral of vorticity ($\boldsymbol{\omega}$) on a surface S using the Stokes' theorem,[14-18]

$$\Gamma = \iint_S \boldsymbol{\omega} dS \tag{1}$$

where $\boldsymbol{\omega} = \nabla \times \boldsymbol{v}$ is the vorticity vector in each point of S, defined as the curl of the velocity vector $\boldsymbol{v}$. Using a tetrahedral FE mesh of a region of interest (Figure 1A), the vorticity was obtained in a 3D domain using a computational framework based on a FE analysis described previously[19] (Figure 1B). Then, to automatically generate a set of 2D surface along the entire vessel of interest, we applied a validated method based on the Laplace algorithm,[13] which gave a set of surfaces, namely S, where the circulation was calculated. Using the solution d obtained by the Laplace algorithm, we calculated the axial unit vector $\boldsymbol{a}$ (Figure 1C) in each node of the tetrahedral FE mesh using:

$$\boldsymbol{a} = \frac{\nabla d}{|\nabla d|} \text{ in } \Omega \tag{2}$$

where d represented a steady state distribution in the domain Ω (vessel of interest) with prescribed values in the inlet ($d = 0$) and outlet ($d = 1$ of the vessel. Then we calculated the projection of the vorticity over a as $\omega_a = \boldsymbol{\omega} \cdot \boldsymbol{a}$. Finally, the circulation Γ was calculated as the spatial integral of the

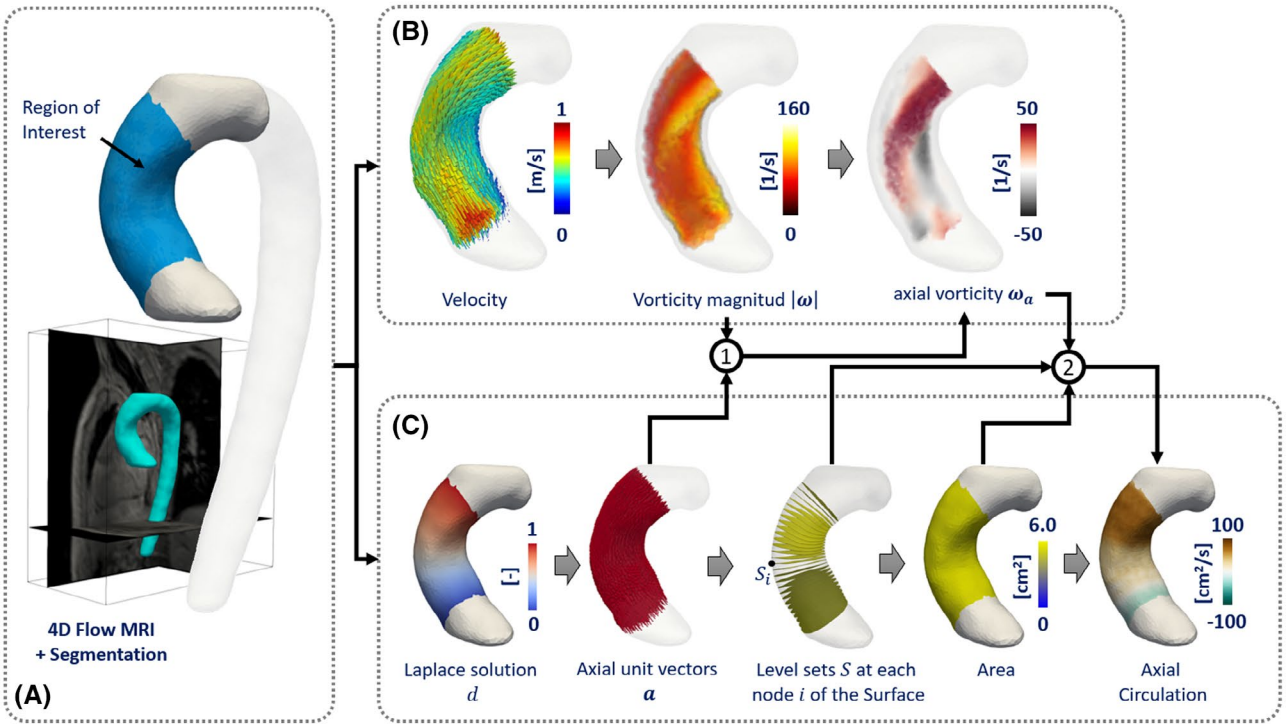

FIGURE 1 Steps of the proposed quantification process. A, The segmentation and boundary condition assignment of the vessel of interest. B, FE process used to calculate the vorticity. C, FE process to calculate the Laplace equation and circulation. From the 4D flow MRI acquisition, a semiautomatic segmentation of the aorta was generated and transformed into a tetrahedral mesh (only the ascending aorta was analyzed). Then, the velocity values were interpolated from the 4D flow data to each node of the mesh, and the vorticity was calculated. Using the Laplace solution, we calculated the axial projection of vorticity as the dot product between axial unit vectors and the vorticity vectors (1). Finally, the axial circulation (Γ_a) was calculated as the spatial integral of the axial projection of vorticity in each level set generated at each node in the surface of the region of interest (2)

ω_a in each level set S generated for each node of the surface mesh using the Laplace solution (see Figure 1C). In this manuscript, we defined this parameter as axial circulation (Γ_a), since it does not only provide information about the rotation of the fluid locally but also allows us to differentiate the helical behavior flow along the vessel with the three-dimensional representation.

2.2 | In-silico analysis

To assess the robustness of our method and its convergence in three dimensions, we performed an in silico experiment using an arch model generated and meshed in ANSYS 2021 R1 (ANSYS Inc, Canonsburg, PA) (Figure 2A). The velocity at radius r and length l (Figure 2B) was assigned using a combination of the Poiseuille flow and Lamb-Oseen equation[19] given by,

$$v(r, l) = \left(\frac{\Delta P}{4\mu L}\left(R^2 - r^2\right)\right)\boldsymbol{a} + \left(\frac{\Gamma(l)}{2\pi r}\left(1 - e^{\frac{-r^2}{k}}\right)\right)\boldsymbol{c} \quad (3)$$

$$\Gamma(l) = 0.5\pi h \sin\left(\frac{3\pi}{L}l\right) \quad (4)$$

where ΔP is the pressure difference assigned as $15[Pa]$, the viscosity $\mu = 0.004\,[Pas]$, L is the total length of the geometry $\pi * 0.03\,[m]$, R is the total radius of the vessel $0.01\,[m]$ and the constants $k = 5e^{-6}$ and $h = 0.01$, $\boldsymbol{a}$ is the axial unit vector and $\boldsymbol{c}$ is the circumferential unit vector in each point of the geometry. Finally $\Gamma(l)$ is the analytical circulation along the geometry used as reference, see Figure 2C.

We performed two experiments to evaluate the robustness and convergence of our method. The first experiment used five different tetrahedral mesh resolutions (Figure 2D) with characteristic lengths of 1.0, 1.5, 2.0, 2.5, 3.0 mm and volumes of 0.12, 0.40, 0.94, 1.84, 3.18 mm^3, respectively. In each node of the tetrahedral mesh, we assigned the analytical velocity value obtained with Equation (3). We added white Gaussian noise to these velocities with SDs of 2.5%, 5.0%, 7.5%, and 10% of the analytical peak velocity. Then we calculated the Γ_a with the process described in Figure 1B,C. Furthermore, we performed a second experiment generating five volumetric images with an isotropic voxel resolution of 1.0, 1.5, 2.0, 2.5, 3.0 mm and volumes of 1.00, 3.38, 8.00, 15.63, 27.00 mm^3, respectively (Figure 2E), in each voxel located inside the geometry, we assigned the analytical values of the velocity using

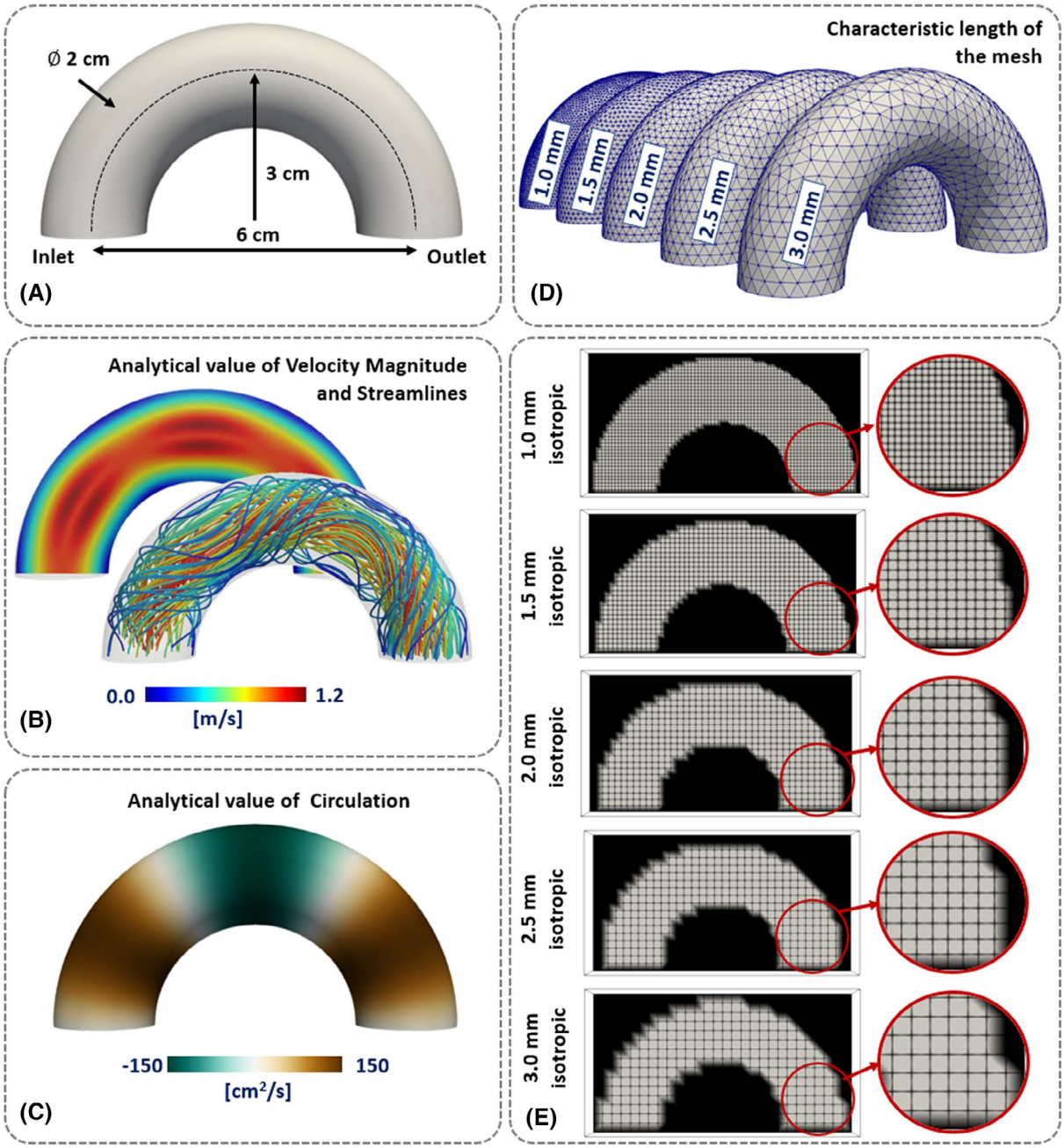

FIGURE 2 A, The arch model used to validate the proposed method. B, the velocity field generated by the Equation (3). C, The analytical value of circulation calculated using the Equation (4). In D, five different mesh resolutions and in E, five different image resolutions used to evaluate the convergence and robustness of the proposed method

the Equation (3). We also added white Gaussian noise with SDs of 2.5%, 5.0%, 7.5%, and 10% of the peak velocity. Then, we interpolated the velocity field from each volumetric image, with or without noise, into each tetrahedral FE mesh described in Figure 2D. Finally, using these meshes, we calculated Γ_a for each case.

Additionally, to compare our method against the standard 2D method described by Hess, et al[15] Bissel, et al[16,17] and Hattori, et al,[18] we reformatted the volumetric images described in the (Figure 2E) into 2D slices, using as reference the coordinates of each point in the surface of each tetrahedral mesh (Figure 2D). Using this process, we compare the FE method with the standard 2D method in the same positions. The normal vector was calculated using the centerline, and the analytical velocity was transferred to the 2D slice using cubic interpolation. For each 2D slice, we used the same volumetric image resolution. Then, the vorticity was calculated using central differences ω_d, and the circulation for the standard 2D method Γ_{2D} was evaluated using the Equation (1).

2.3 | In vivo MR analysis

To show the clinical applicability of our method, we used retrospective 4D flow MRI data from six healthy volunteers (five males, mean age 30.5 ± 5 y old) and six BAV patients (4 males, mean age 25.5 ± 10 y old), three with right- and three with left-handed flow. The volunteer data were acquired in a clinical 3T Philips MR scanner (Achieva, Philips Healthcare, Best The Netherlands) and the patient data using a clinical 3T Trio SIEMENS MR scanner (Healthcare, Erlangen, Germany). The volumetric acquisition included the entire thoracic aorta acquired in sagittal orientation, without administration of gadolinium contrast, performed with retrospective (Philips) / prospective (SIEMENS) ECG gating and respiratory navigator. Imaging parameters for the 4D flow MRI data obtained with 3T Philips MR scanner were as follows: voxel size = 2.2 × 2.2 × 2.5 mm, number of cardiac phases: 25, TE = 2.7 ms, repetition time = 4.8 ms, flip angle = 5°, VENC = 200 cm/s. Scan times for 4D flow CMR were typically around 16 min/scan. For the 4D flow, MRI data obtained with 3T Trio SIEMENS scanner were as follows: voxel size = 1.7 × 2.0 × 2.2 mm, number of cardiac phases: 10 across systole, TE = 40 ms, repetition time = 5.1 ms, flip angle = 7°. The velocity encoding range was determined using the lowest nonaliasing velocity on scout measurements. Scan times for 4D flow CMR were typically around 10-15 min/scan. To assess the differences between healthy volunteers and BAV patients, we computed the mean value and SD of the axial circulation in the ascending aorta. The study was approved by the local ethics committee, and informed consent was obtained from all participants.

2.4 | Segmentation, mesh generation, and quantification process

The 4D Flow MRI data sets were processed using an in-house MATLAB toolbox (MathWorks, Natick, MA, USA),[20] whose functionalities allow the segmentation of the thoracic aorta generation of a FE mesh. To process the 4D Flow MRI data, we created an angiographic image ($I^{PC\text{-}MRI}$) using the algorithm proposed by Bock et al.[21] These images were segmented using a semiautomatic process based on thresholding, labeling, and manual separation adjustment (Figure 1A). From the final segmented vessel, we generated a tetrahedral mesh using the iso-2mesh MATLAB toolbox.[22] Following, we transferred the velocity vector of 4D flow MRI data sets to the nodes of the FE mesh. Then, 3D maps of vorticity vector field were calculated using the FE algorithm described by Sotelo et al[19] (Figure 1B). Once the vorticity was obtained, we prescribed the boundary conditions on the tetrahedral FE mesh to obtain the Laplace solution,[13] and the axial circulation was automatically calculated with the procedure described in Figure 1C. All results were analyzed and visualized using the scientific visualization software Paraview (Kitware Inc., Clifton Park, New York, USA).

2.5 | Statistical analysis

In the in-silico analysis, all results of Γ_a and Γ_{2D} were compared with the analytical values Γ obtained by the Equation (4) using the mean absolute error (*MAE*) as

$$MAE = \frac{\sum_{i=1}^{N} \left|\Gamma - \Gamma'\right|}{N} \tag{5}$$

where N denotes the number of nodes along the vessel wall. We also analyze the Pearson correlation, Bland-Altman and correlation plots plot using th absolute values of the analytical circulation $|\Gamma|$ and the estimated value of circulations $|\Gamma_a|$ and $|\Gamma_{2D}|$. To assess the results from in vivo experiments, we computed the mean value and SD of the axial circulation at peak systole in the AAo. Additionally, we performed the Mann-Whitney test at a 5% significance level to detect statistically significant differences between groups.

3 | RESULTS

3.1 | In-silico analysis

For experiment 1, in the absence of noise, the Γ_a computed in 3D converged toward the analytical values as the characteristic length of the elements decreases (see Figure 3A). The *MAE* was less than 10 cm^2/s subjected to different noise levels and mesh resolutions, underestimating the axial circulation relative to the analytical value. In Figure 3B, we show 3D maps for the tetrahedral finite element mesh with a characteristic length of 2.0 mm (see Figure 3A, dashed line), and no significant variations were observed on the axial circulation maps.

In experiment 2, we showed the results of the simulated volumetric images with different resolutions and in the absence of noise and four different noise levels. The results of Γ_a in these geometries are shown in Figure 4A. The *MAE* was less than 45 cm^2/s in all cases, providing greater precision in high resolution images, compared to low resolution images. Similarly to experiment 1, the axial-circulation was not significantly affected by noise. Interestingly, for image resolutions larger than 2 mm, the use of finer meshes slightly increased the error in the quantification of Γ_a. Furthermore, the low resolution image (isotropic voxel 3 mm) showed an improved

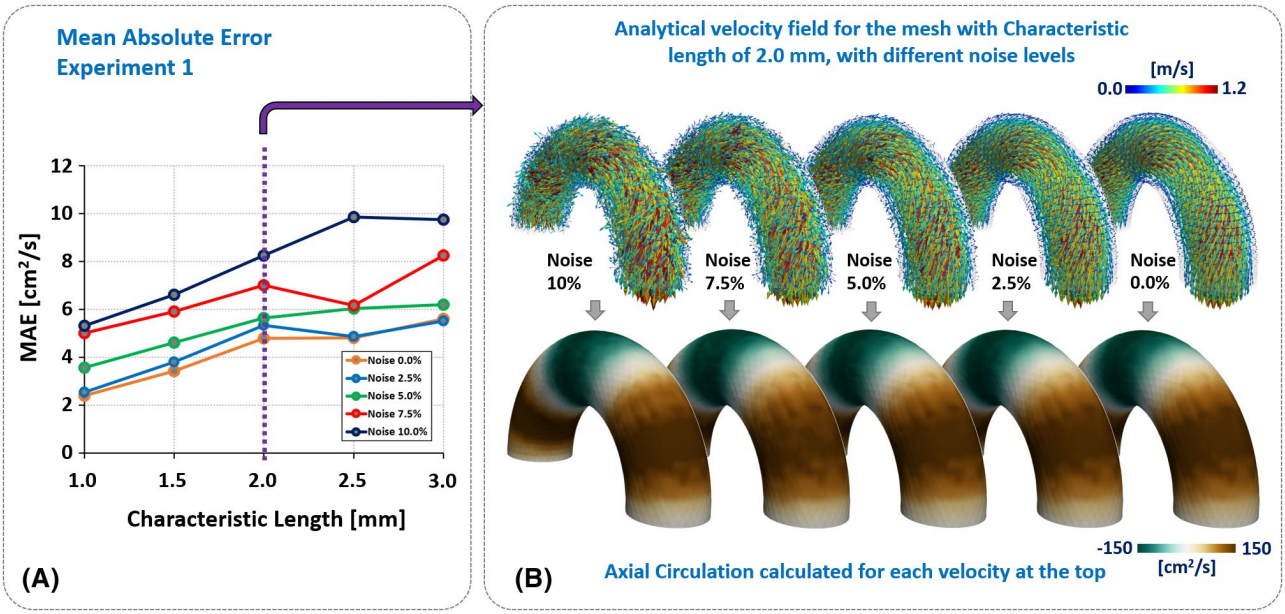

FIGURE 3 Results from experiment 1. A, *MAE* for different mesh resolutions and noise levels. In B, we show the result of the velocity vector field and axial-circulation for a characteristic length of the element of 2 mm, and different noise levels (dashed line in A)

quantification of Γ_a compared to the higher resolution images (isotropic voxel 1 mm). Comparing our finite element results with the standard 2D method using the centerline of the geometry, we observed that the standard 2D method is also stable compared with the tested image resolutions and noise levels, but the values of the estimated circulation (Γ_{2D}) were underestimated (range $\pm$80 cm^2/s) below the Γ_a values obtained with FE (range $\pm$110 cm^2/s) when compared to the analytical values (range $\pm$ 157 cm^2/s).

In the Supporting Information Table S1 which is available online, we include the Pearson correlation comparing the analytical value of circulation Γ with the value obtained by our finite element method Γ_a and the standard 2D method Γ_{2D}, for different image resolutions, mesh sizes and noise levels. For all cases the Pearson correlation was greater than 0.95. Moreover, in the Supporting Information Figures S1 and S2, we show the Bland-Altman plots and correlation plots between the analytical value of circulation Γ, and the value obtained by our finite element method Γ_a (for different image resolutions and mesh sizes) and the standard 2D method Γ_{2D} (for different image resolutions), the noise level was grouped, because Figure 4 shows that both method are insensitive to noise.

From the Bland-Altman we overserved a subestimation of circulation values for Γ_a and Γ_{2D} in comparison with the analytical values Γ, with less variability in Γ_a. The bias ranged between 44.00 cm^2/s to 18.53 cm2/s, for Γ_a and between 55.42 cm^2/s to 53.91 cm^2/s, for Γ_{2D}. For larger mesh sizes combined with lower image resolution we observed more variability in the results.

From the correlation plots, a greater loss of slope in the standard 2D method Γ_{2D} than in our finite element method Γ_a was observed. In our method, the slope ranged between 0.57 to 0.82, and the R^2 between 0.94 to 0.99, for the case of the standard 2D method the slope ranged between 0.46 to 0.48, and the R^2 between 0.95 to 0.98. Both methods showed high precision but our method showed greater accuracy.

3.2 | In vivo MR analysis

The axial circulation (mean $\pm$ SD) of the healthy volunteer group was 13.83 $\pm$ 28.78 cm^2/s, in BAV patients with right-handed flow 724.37 $\pm$ 317.53 cm^2/s, and BAV patients with left-handed flow −480.99 $\pm$ 387.29 cm^2/s (Figure 5). There were significant differences between healthy volunteers and BAV patients groups (*P*-value of .000022), and also between BAV patients with a right-handed helical flow and healthy volunteers (p-value of 0). The same p-value was obtained between the groups of BAV patients with left-handed helical flow and healthy volunteers. The group of BAV patients showed a considerable range of axial circulation [cm^2/s] data, interquartile range [Q1 | Q3] of axial circulation for the group of healthy volunteers were [−4.0 | 37.1] cm^2/s, and BAV patients with s right-handed flow [363.4 | 960.6] cm^2/s and BAV patients with left-handed flow [−891.4 | 121.9] cm^2/s. From a qualitative point of view, in Figure 5 we observe that the magnitude of axial circulation for the group of BAV patients with right-handed flow, is over 50 times

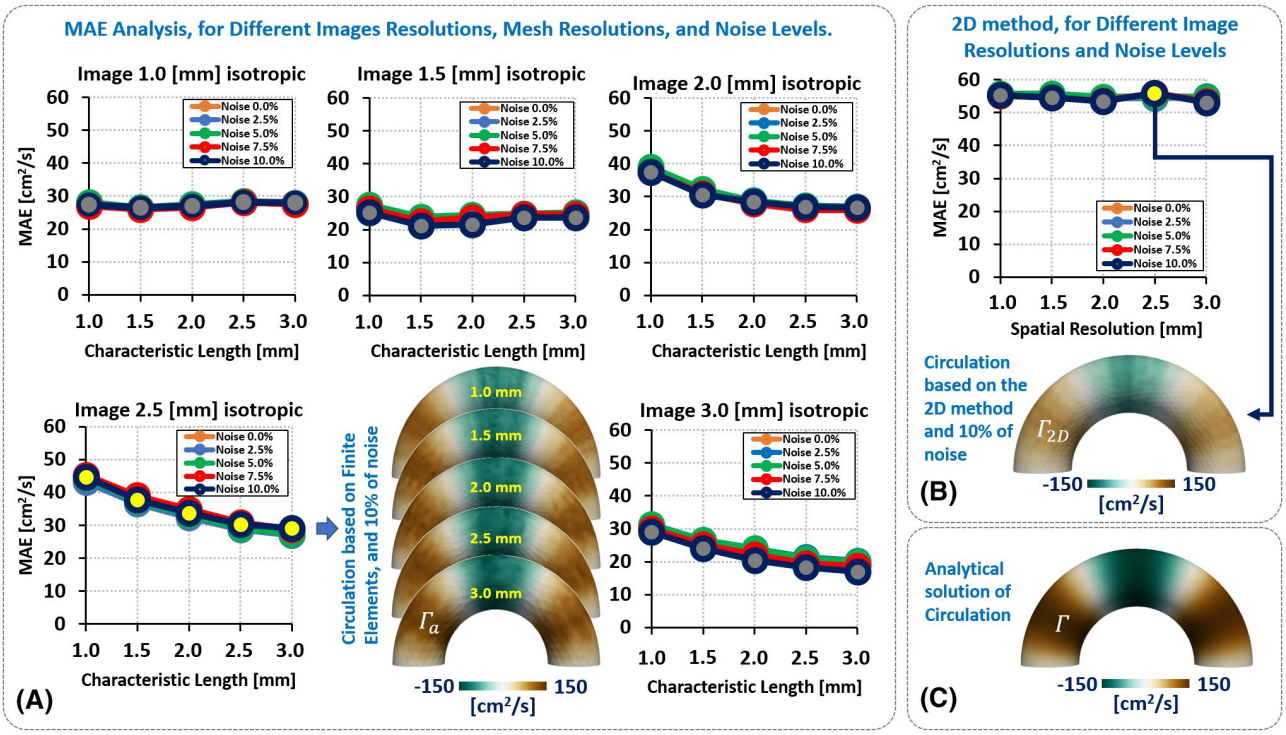

FIGURE 4 Results from experiment 2. A, *MAE* for different mesh resolutions and noise levels of the velocity field interpolated from the volumetric images, with different spatial resolution, we also show the 3D maps of Γ_a for five different meshes and 10% of noise level, obtained from the image with a spatial resolution of 2.5 mm. In B, we show the *MAE* for the volumetric images showed in Figure 2E with five different noise levels; we also show the 3D maps of Γ_{2D} for the image with a spatial resolution of 2.5 mm and 10% of noise level (The three-dimensional maps of Γ_{2D} was created using a 2D slice for each node of the surface mesh). In C, we show the analytical solution of circulation using Equation (4)

greater than the magnitude of axial circulation in healthy volunteers. Also, in the group of BAV patients with left-handed flow, the magnitude of axial circulation is over 34 times greater than the magnitude of axial circulation in healthy volunteers. On the group of BAV patients, two of them showed the bigger values of axial circulation for right- and left-handed flow directions, the right- handed flow direction patient shown a mean value of 960 cm^2/s and the left- handed flow direction patient shown a mean value of −891 cm^2/s.

4 | DISCUSSION

We proposed a method to calculate the circulation on a 3D domain that we called axial-circulation. This method allowed us to evaluate local rotations and helical behavior of the blood flow in the ascending aorta of BAV patients using the 3D maps obtained from 4D flow MRI data using a finite element approach.

Our method has distinctive advantages over current 2D formulations. It includes the automatic generation of 3D maps without generating overlapping planes[13] as it does not rely on precise centerline calculation for plane detection, making it helpful to work with complex geometries. The first in silico experiments using the Equations (3) and (4) showed that our 3D formulation produces precise and accurate approximations for the axial circulation. In the absence of noise, they converge to the analytical values as the characteristic length of the elements becomes small. Also, the method showed robustness to noise in in-silico experiments.

From the in silico analysis, the axial circulation predicted by our FE formulation induces less error than that obtained from the standard 2D formulation. The *MAE* obtained by both methods showed negligible variation for different noise levels. However, the difference of circulation obtained by our 3D formulation was below 45 cm^2/s, with the higher level of noise. On the other hand, the error incurred by the 2D method was around 55 cm^2/s for different noise levels. Our method showed a good precision in estimating the circulation, in images with higher spatial resolution, similarly to the 2D method (Figure 4). However, in the case of lower resolution images, the precision was affected by the characteristic length of the tetrahedral element used, mainly due to a larger number of mesh nodes inside of a single voxel, affecting the quantization of the spatial derivatives of velocity, which directly

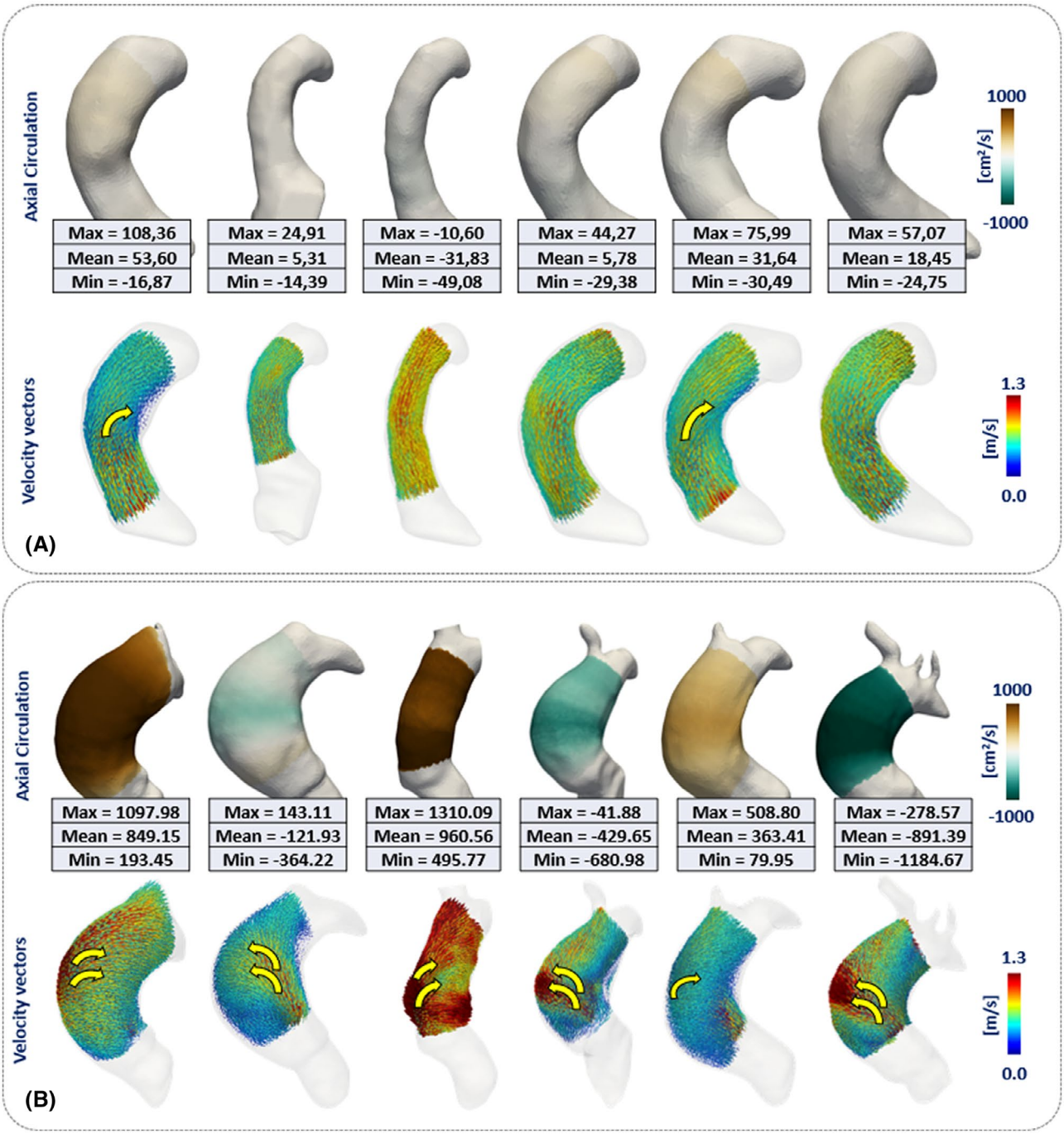

FIGURE 5 A, Axial circulation maps and velocity vector field in the AAo for each healthy volunteer (we also show the max, mean, and min values of axial circulation). B, Axial circulation maps and velocity vector field in the AAo for each BAV patient (we also show the max, mean, and min values of axial circulation). Additionally, with yellow arrows, we show the direction of the velocity vectors in healthy volunteer and BAV patients

affects the quantization of the circulation. Nevertheless, all the results obtained by our method showed less error than the standard 2D method (see Supporting Information Figures S1 and S2).

The in vivo results showed that axial-circulation is an interesting parameter for evaluating rotational and helical flow in complex geometries. There were noticeable differences between the axial circulation of BAV patients, and healthy volunteers explained primarily by the flow pattern in the ascending aorta of BAV patients, as there was a helical flow that rises until the aortic arch (Figure 5). These atypical flow patterns may alter the biomechanics of the vessel, potentially causing remodeling of the vessel in the region exposed to this helical flow. This is also supported by the work developed by Bissel, et al[16] and Hattori, et al.[18]

For healthy volunteers and BAV patients, we found a statistically significant (*P*-value of 0.000022) difference in the axial-circulation in the ascending aorta, consistent with the difference of eccentricity and circumferential wall shear stress reported by other authors.[10-13] The main advantage of the proposed FE method is the analysis of axial-circulation on the entire vessel surface. The clinical implications of more accurate and precise predictions of the axial-circulation may play an essential role in disease genesis and progression. In the study of Bissel, et al,[16] the authors demonstrate that the left-handed flow pattern show more severe abnormalities than right-handed, which may require ascending aortic replacement at a younger age. Our method could facilitate risk stratification in BAV aortopathy, predicting these flow abnormalities at an early stage.

One limitation of the proposed methodology is that our methodology can evaluate only one vessel of interest without any branches. We also found this limitation when we used the centerline method to generate 2D slices. Using any of both methods, each branch in the vessel would need to be analyzed independently. If branching vessels are required in the data analysis, we could perform a semiautomatic process to select the inlet and outlet nodes for each branch vessel. We will include the supra-aortic vessels in our model in future research, modifying our Laplacian approach. Additionally, larger number of participants and longitudinal follow-up data are needed to correlate axial-circulation with clinical outcomes.

In conclusion, we propose a novel 3D formulation and a computational method to estimate the axial-circulation in a vessel, which can be used to assess the differences between normal and diseased hemodynamic from 4D-Flow MRI data. This method also correctly differentiated between the visually seen right- and left-handed helical flow, which shows the clinical feasibility of the presented methodology. However, longitudinal studies in a large cohort of patients may provide more clinical insight about the use of this parameter.

ACKNOWLEDGMENT

This publication was funded by ANID – Millennium Science Initiative Program – NCN17_129. Also, has been supported by CONICYT-FONDECYT Postdoctorado #3170737, the ANID Ph. D. Scholarship #21170592, and ANID FONDECYT de Iniciación en Investigación #11200481 and ANID FONDECYT #1181057.

DATA AVAILABILITY STATEMENT

Access to our 4D Flow Matlab Toolbox is available from https://github.com/JulioSoteloParraguez/4D-Flow-Matlab-Toolbox

ORCID

Julio Sotelo https://orcid.org/0000-0002-0915-5215
Malenka M. Bissell https://orcid.org/0000-0002-1282-2859
Hernan Mella https://orcid.org/0000-0001-8712-146X
Joaquín Mura https://orcid.org/0000-0003-1157-1602

REFERENCES

1. Borger MA, Fedak PWM, Stephens EH, et al. The American Association for Thoracic Surgery consensus guidelines on bicuspid aortic valve-related aortopathy: full online-only version. *J Thorac Cardiovasc Surg*. 2018;156:e41-e74.
2. Itagaki S, Chikwe JP, Chiang YP, Egorova NN, Adams DH. Long-term risk for aortic complications after aortic valve replacement in patients with bicuspid aortic valve versus Marfan syndrome. *J Am Coll Cardiol*. 2015;65:2363-2369.
3. Siu SC, Silversides CK. Bicuspid aortic valve disease. *J Am Coll Cardiol*. 2010;55:2789-2800.
4. Evangelista A, Gallego P, Calvo-Iglesias F, et al. Anatomical and clinical predictors of valve dysfunction and aortic dilation in bicuspid aortic valve disease. *Heart*. 2018;104:566-573.
5. Cavalcante JL, Lalude OO, Schoenhagen P, Lerakis S. Cardiovascular magnetic resonance imaging for structural and valvular heart disease interventions. *JACC Cardiovasc Interv*. 2016;9:399-425.
6. Whitlock MC, Hundley WG. Noninvasive imaging of flow and vascular function in disease of the aorta. *JACC Cardiovasc Imaging*. 2015;8:1094-1106.
7. Edlin J, Youssefi P, Bilkhu R, et al. Haemodynamic assessment of bicuspid aortic valve aortopathy: a systematic review of the current literature. *Eur J Cardiothorac Surg*. 2019;55:610-617. PMID: 30239633.
8. Guzzardi DG, Barker AJ, van Ooij P, et al. Valve-related hemodynamics mediate human bicuspid aortopathy: insights from wall shear stress mapping. *J Am Coll Cardiol*. 2015;66:892-900.
9. Bollache E, Guzzardi DG, Sattari S, et al. Aortic valve-mediated wall shear stress is heterogeneous and predicts regional aortic elastic fiber thinning in bicuspid aortic valve-associated aortopathy. *J Thorac Cardiovasc Surg*. 2018;156:2112-2120.e2.
10. Sigovan M, Hope MD, Dyverfeldt P, Saloner D. Comparison of four-dimensional flow parameters for quantification of flow eccentricity in the ascending aorta. *J Magn Reson Imaging*. 2011;34:1226-1230.
11. Garcia J, Barker AJ, Murphy I, et al. Four-dimensional flow magnetic resonance imaging-based characterization of aortic morphometry and haemodynamics: impact of age, aortic diameter, and valve morphology. *Eur Heart J Cardiovasc Imaging*. 2016;17:877-884.
12. Rodríguez-Palomares JF, Dux-Santoy L, Guala A, et al. Aortic flow patterns and wall shear stress maps by 4D-flow cardiovascular magnetic resonance in the assessment of aortic dilatation in bicuspid aortic valve disease. *J Cardiovasc Magn Reson*. 2018;20:28.
13. Sotelo J, Dux-Santoy L, Guala A, et al. 3D axial and circumferential wall shear stress from 4D flow MRI data using a finite element method and a laplacian approach. *Magn Reson Med*. 2018;79:2816-2823.

14. Bouno PL. *Advanced Calculus: Differential Calculus and Stokes' Theorem*. Berlin, Germany: De Gruyter; 2016.
15. Hess AT, Bissell MM, Glaze SJ, et al. Evaluation of circulation, Γ, as a quantifying metric in 4D flow MRI. *J Cardiovasc Magn Reson*. 2013;15:E36.
16. Bissell MM, Hess AT, Biasiolli L, et al. Aortic dilation in bicuspid aortic valve disease: flow pattern is a major contributor and differs with valve fusion type. *Circ Cardiovasc Imaging*. 2013;6:499-507.
17. Bissell MM, Loudon M, Hess AT, et al. Differential flow improvements after valve replacements in bicuspid aortic valve disease: a cardiovascular magnetic resonance assessment. *J Cardiovasc Magn Reson*. 2018;20:10.
18. Hattori K, Nakama N, Takada J, et al. Bicuspid aortic valve morphology and aortic valvular outflow jets: an experimental analysis using an MRI-compatible pulsatile flow circulation system. *Sci Rep*. 2021;11:2066.
19. Sotelo J, Urbina J, Valverde I, et al. Three-dimensional quantification of vorticity and helicity from 3D cine PC-MRI using finite-element interpolations. *Magn Reson Med*. 2018;79:541-553.
20. Sotelo J, Mura J, Hurtado D, Uribe S. A novel MATLAB toolbox for processing 4D Flow MRI data. *Proc Intl Soc Mag Reson Med*. 1956;27:2019.
21. Bock J, Frydrychowicz A, Stalder AF, et al. 4D phase contrast MRI at 3 T: effect of standard and blood-pool contrast agents on SNR, PC-MRA, and blood flow visualization. *Magn Reson Med*. 2010;63:330-338.
22. Qianqian F, Boas DA. Tetrahedral Mesh Generation from Volumetric Binary and Gray-Scale Images. In Proceedings of the 6th IEEE International Conference on Symposium on Biomedical Imaging: From Nano to Macro, Boston, Massachusetts, USA, pp. 1142-1145.

SUPPORTING INFORMATION

Additional Supporting Information may be found online in the Supporting Information section.

FIGURE S1 Bland-Altman plots, between the analytical value of circulation Γ and the proposed three-dimensional value based on finite elements Γ_a, and the standard 2D method Γ_{2D}, for different mesh resolutions, noise levels and image resolution

FIGURE S2 Linear regression plots, between the analytical value of circulation Γ and the proposed three-dimensional value based on finite elements Γ_a, and the standard 2D method Γ_{2D}, for different mesh resolutions, noise levels and image resolution

TABLE S1 Pearson correlation between the analytical circulation Γ and the proposed axial circulation Γ_a (for different noise levels, mesh resolutions and image resolutions), and the standard 2D method Γ_{2D} (for different noise levels and image resolutions)

How to cite this article: Sotelo J, Bissell MM, Jiang Y, Mella H, Mura J, Uribe S. Three-dimensional quantification of circulation using finite-element methods in four-dimensional flow MR data of the thoracic aorta. *Magn Reson Med*. 2022;87:1036–1045. https://doi.org/10.1002/mrm.29004